1992

Preliminary Analysis of ERS-1 SAR for Forest Ecosystem Studies

Terry L. Sharik

Preliminary Analysis of ERS-1 SAR for Forest Ecosystem Studies

M. Craig Dobson, *Senior Member, IEEE*, Leland Pierce, *Member, IEEE*, Kamal Sarabandi, *Member, IEEE*, Fawwaz T. Ulaby, *Fellow, IEEE*, and Terry Sharik

Abstract— **In this paper we examine an image obtained by the *C*-band VV-polarized ERS-1 SAR with respect to potential land applications. A scene obtained near noon on Aug. 15, 1991 along the U.S.–Canadian border near Sault Ste. Marie is calibrated relative to an array of trihedral corner reflectors and active radar calibrators distributed across the swath. Extensive contemporaneous ground observations of forest stands are used to predict σ° at the time of the SAR overpass using a first-order vector radiative transfer model (MIMICS). These predictions generally agree with the calibrated ERS-1 data to within 1 dB. It is demonstrated that the dynamic range of σ° is sufficient to perform limited discrimination of various forest and grassland communities even for a single-date observation. Furthermore, it is demonstrated that retrieval of near-surface soil moisture is feasible for grass-covered soils when plant biomass is less than 1 tonne/ha.**

I. Introduction

The first European Remote Sensing satellite (ERS-1) was launched into space by Arianne V44 on July 17, 1991. Launched into a near-polar orbit, ERS-1 provides 3-day repeat coverage of specific tracks during its initial 3-month commissioning phase. The ERS-1 carries a suite of instruments which includes a *C*-band (5.3 GHz) synthetic aperture radar (SAR). While primarily designed for observation of ocean processes and polar ice regions, the SAR has great potential for terrestrial observations as has been demonstrated by *L*-band SAR's on Seasat [1], [2] and the Shuttle Imaging Radars, SIR-A and SIR-B [2]–[6].

The strengths of SAR as a land observation tool reside in (1) the sensitivity of radar backscatter to the moisture content of terrain media and the geometrical parameters of the scatterers in the media (i.e., size, shape, roughness, and orientation) and (2) an all-weather, day or night imaging capability. The provision of a 3-day repeat interval by the ERS-1 SAR presents a unique opportunity to monitor changes in land-surface and land-cover characteristics over both short and long time intervals. The *C*-band ERS-1 SAR with VV polarization and 23° angle of incidence is particularly well suited for monitoring changes in near-surface soil moisture for regions with short vegetation cover (such as grasses) and also the structural characteristics of taller vegetation covers with greater biomass (such as forests).

The purpose of the current study is to examine the utility of ERS-1 SAR data for studies of forest ecosystems. Multitemporal observations over several annual cycles will be required to fully achieve this purpose. In the interim, the initial image data obtained by the ERS-1 SAR is evaluated with respect to discrimination of various land-cover categories and forest communities. This report will focus upon an ERS-1 SAR scene obtained on Aug. 15, 1991 along a portion of the ecotone between the boreal forest and northern temperate forest communities and located near Sault Ste. Marie at the border of Canada and the U.S.

This scene has been processed and externally calibrated using an array of point targets distributed across the image swath. The radar backscattering coefficients σ° averaged over 4-ha forest stands are compared with theoretical expectations based upon a first-order, vector radiative transfer model for forest canopies (MIMICS) as driven by contemporaneous ground data acquisitions. In addition, the image statistics for various nonforest and forest land-cover categories are examined with respect to separability in σ°. The response of the ERS-1 SAR to spatial variation in near-surface soil moisture is also examined for grass-covered surfaces.

II. ERS-1 SAR Data

The test site for this study (46°20′ N. latitude, 84°50′ W. longitude) lies at the intersection of ascending and descending tracks for the ERS-1 SAR, as shown in Fig. 1. This location provides the opportunity for 3-day repeat coverage during the ERS-1 commissioning phase with imaging opportunities at 12:28 (EDT) on the descending pass and again 11 h later at 23:47 (EDT) on the ascending pass. During the initial test period of the SAR, a large number of both ascending and descending scenes were acquired for this site by the Gatineau receiving station. To date, only the scene acquired on orbit 424 at 12:28 (EDT) on Aug. 15, 1991 has been processed. This scene was processed at Gatineau to a six-look product. This scene is shown in Fig. 2. For the purpose of illustration, it is not shown at full resolution. It is resampled using a 6×6 boxcar filter and decimated to 1366×1366 pixels.

This test site is one of many being used to evaluate the calibration of the ERS-1 SAR. An array of point targets with known radar cross-section are distributed along a 45-km transect in the range direction. The calibration targets include both passive trihedral corner reflectors (243.8 cm orthogonal

Manuscript received June 1, 1991; revised September 26, 1991. This work was supported by the National Aeronautics and Space Administration under Grant NAGW 1362.

Radiation Laboratory Electrical Engineering and Computer Science The University of Michigan, Ann Arbor, MI 48109
School of Forestry and Wood Products Michigan Technological University, Houghton, MI 49931

IEEE Log Number 9105847.

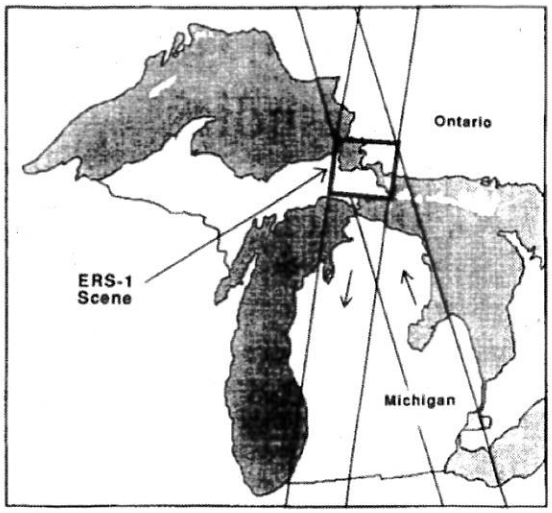

Fig. 1. Positions of ERS-1 image swaths over Michigan during the commissioning phase and the location of the ERS-1 scene.

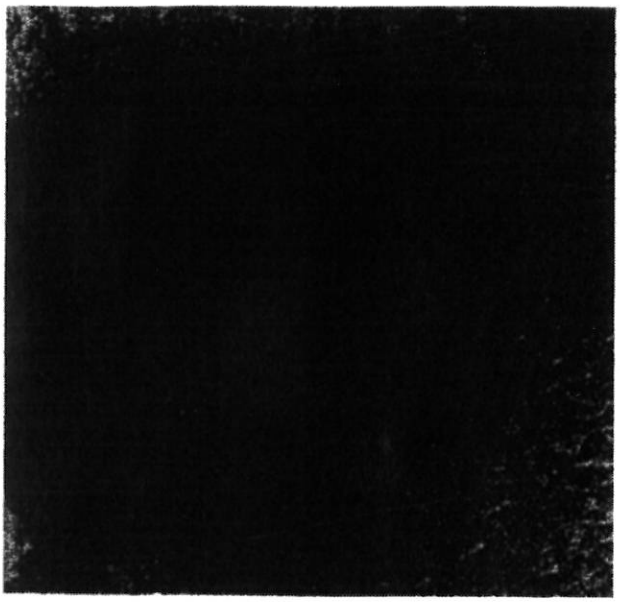

Fig. 2. ERS-1 SAR image of Sault Ste. Marie acquired on orbit 424 at 12:28 EDT on Aug. 15, 1991 copyright ERS-1-R ESA, 1991. The box shows the area included in Fig. 7.

leg length) and active radar calibrators [7]. All targets are boresighted to the ERS-1. All targets have cross-sections of greater than 46 dB m^2 and are located on flat surfaces of concrete or short grass. Hence, in all cases the signal to background ratio is greater than 30 dB. A typical example of the point target response to one of the trihedral corner reflectors is shown in Fig. 3.

Absolute calibration of the ERS-1 SAR data via the radar equation entails both internal and external calibration components. The internal component requires knowledge of transmit power, receiver, and processing gains as well as angular dependent quantities such as range and antenna gain. Most of this information is not available for this preliminary ERS-1 scene. The external calibration component requires one (or

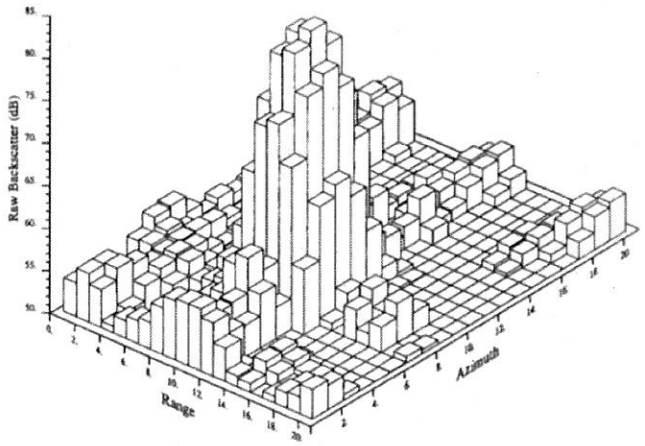

Fig. 3. ERS-1 SAR response to a 243.8-cm trihedral corner reflector located on a concrete apron.

more) point or distributed targets of known radar cross-section and also knowledge of the number of independent looks and resolution (range and azimuth).

For the six-look ERS-1 scene, each digital number DN is proportional to the received voltage. Hence, image intensity $I(I = 20 \log DN)$ is the product of any processor gain G_p and received power P, i.e.,

$$I = G_p P. \tag{1}$$

For an area-extended target, the mean received power is given by

$$\bar{P} = \bar{P}_s + \bar{P}_n \tag{2}$$

where $\bar{P}_s$ = mean power received from the target and $\bar{P}_n$ is the mean receiver noise power. The radar equation relates $\bar{P}_s$ to the radar backscattering coefficient σ° of a given target.

$$\bar{P}_s = \frac{P_t G^2 \lambda^2 \sigma^\circ A_i}{(4\pi)^3 R^4} \tag{3}$$

P_t is the transmit power, G is antenna gain, λ is wavelength, A_i is the illuminated area, and R is range.

For a calibration point target, the radar equation becomes

$$P_{s_c} = \frac{P_t G^2 \lambda^2 (\sigma_c + \sigma_b^\circ A_i)}{(4\pi)^3 R^4} \tag{4}$$

where σ_c is the radar cross section of the calibration target and σ_b° is the backscattering coefficient of the background. For convenience, let

$$C = \frac{P_t G^2 \lambda^2}{(4\pi)^3 R^4} \tag{5}$$

and hence,

$$P_{s_c} = C(\sigma_c + \sigma_b^\circ A_i). \tag{6}$$

Since $\sigma_c/(\sigma_b^\circ A_i) > 30$ dB for the point calibration targets used in this study, the effects of the background are, henceforth, ignored

$$P_{s_c} = C\sigma_c \tag{7}$$

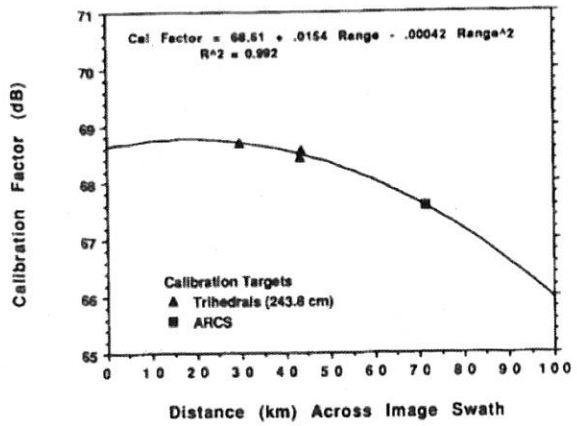

Fig. 4. Preliminary calibration factor established for ERS-1 SAR image of Sault Ste. Marie on orbit 424 on Aug. 15, 1991.

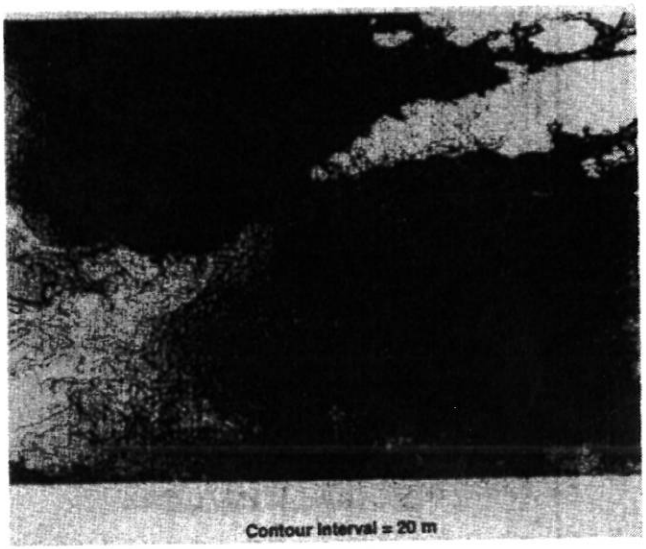

Fig. 5. Topography of the Sault Ste. Marie area from USGS 1° × 2° digital elevation model.

Through substitution, it can be shown that the image intensity of a point calibration target I_c is related to σ_c by

$$\sigma_c = (\frac{I_c}{G_p} - P_n)/C \tag{8}$$

In this case, $\sigma_c \gg P_n$, hence the effects of P_n are negligible and

$$I_c \simeq G_p C \sigma_c \tag{9}$$

The product G_pC is a calibration offset that accounts for system and processing effects and assumes noise to be negligible. This offset is calculated for each calibration target in the ERS-1 scene by integrating I over the main beam and accounting for the six-look summation of the processor.

For an area-extended target with $\bar{P}_s \gg \bar{P}_n$, substitution of (5) into (1) to (3) yields.

$$\sigma^\circ = I/G_pCA_i = I/K \tag{10}$$

where K is a calibration factor which is dependent upon range and incorporates system and processing gains, range losses and illumination area. Note that K is only valid for regions where $\bar{P}_s \gg \bar{P}_n$. The values of K calculated for each point calibration target are plotted versus ground range in Fig. 4. The variation in $K(\theta)$ is the product of antenna gain, R^4 losses and changes in A_i. The local calibration is extended across the ERS-1 swath using the empirical equation shown in Fig. 4:

$$K_\theta(dB) = 68.61 + 0.0154R - 0.00042R^2 \tag{11}$$

III. Forest Test Site

The ERS-1 scene in Fig. 2 covers a transitional region along the ecotone between the northern boreal forests of Canada and the northern temperate forests to the south. The image shows Lake Superior in the upper left, the rough topography of the Canadian Shield in the upper right, and the eastern portion of Michigan's Upper Peninsula in the lower half. The eastern end of the Upper Peninsula of Michigan contains the Luce and Mackinac ecosystem districts [8]. With the exception of beach ridges and moraines, local topographic relief is low. Elevation ranges from 180 m at the lake level of Lake Superior to 300 m on some end moraines. Fig. 5 shows elevation as shaded relief with 20-m contours derived from a U.S. Geological Survey 1° × 2° digital elevation model for the Sault Ste. Marie quadrangle. Areas with elevation ≥ 300 m are coded to white and not contoured in Fig. 5.

The region south of Sault Ste. Marie is dominated by a flat clay plain with small areas of sandy ground moraine and sandy lake plains as shown in Fig. 6. The clayey areas are extensively used for pasture and hay production and appear dark (low backscatter) on the ERS-1 image. The sandy areas are generally forested and consequently show much higher backscatter. West of this area, elevation rises by 25 m to the relatively flat Raco Plain, which is mainly covered by sandy outwash deposits. These sands are droughty and are covered by upland conifers such as jack pines (*Pinus banksiana*) and with red pines (*Pinus resinosa*) and white pines (*Pinus strobus*) on the more moist areas. Poorly drained areas between the Raco Plain and the clay lake plain contain lowland conifers such as black spruce (*Picea mariana*) and white spruce (*Picea glauca*). North of the Raco Plain are moraines with loamy soils which support the growth of northern hardwood stands dominated by beech (*Fagus grandifolia*), sugar maple (*Acar saccharum*) and red maple (*Acer rubrum*). Near the Lake Superior shore are lowland conifer bogs dominated by northern white-cedar (*Thuja occidentalis*). Stands of bigtooth aspen (*Populus grandidentata*) and trembling aspen (*Populus tremuloides*) occur throughout the peninsula as pioneer species after disturbance.

The generalized soil map shown in Fig. 6 is digitized from the Soil Association Map of Michigan [9]. The digital land-cover data shown in Fig. 7 is for 48 km×48 km area comprising 25 townships [10]. Visually, there are obvious correlations between ERS-1 backscatter and elevation, soils and land-cover.

IV. Radar Backscatter from Land-Cover Classes

In order to explore the visual correlation between ERS-1 backscatter and land-cover, the observed σ° is compared to that estimated for land-cover categories using a first-order

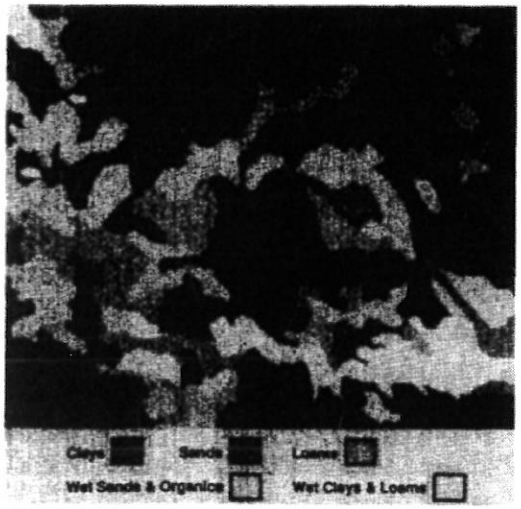

Fig. 6. Generalized soil association map of the eastern end of Michigan's Upper Peninsula [9].

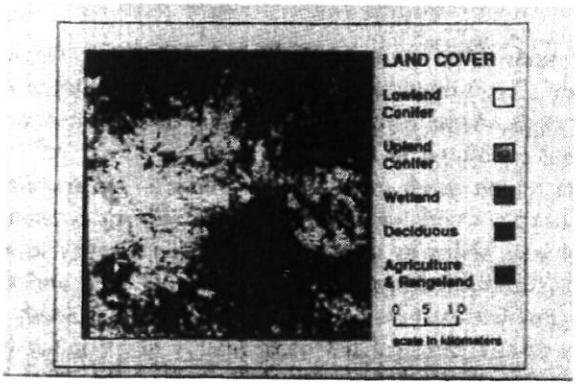

Fig. 7. Land-cover categories for a 25-township area of Michigan's Upper Peninsula [10].

vector radiative transfer model. This model, MIMICS, requires specification of a large number of forest canopy and surface properties [11].

Within this ERS-1 scene, an experimental program has measured sample stands of each forest association. Each sample stand is homogeneous within a minimum area of 200m×200m. Within a stand, 8 randomly located transects contain a total of 40 sampling locations for determination of stem density, tree height, and diameter by species. This represents a 10% sample of the stand for the overstory trees. Leaf area index is determined by optical techniques [12] at the time of the ERS-1 overpass for each stand. In addition, the moisture and dielectric properties of the canopy (trunks, branches and leaves) and the soil are measured using gravimetric techniques and field-portable dielectric probes at C-band. Where necessary, the dielectric properties of foliage and soil are inferred from moisture content using a Debye–Cole dual dispersion model [13] and a semi-empirical model [14], respectively.

A. MIMICS Estimates of Radar Backscatter

A small number of forest stands which could be unambiguously identified on the ERS-1 scene shown in Fig. 2 are selected for simulation of σ° using MIMICS. These

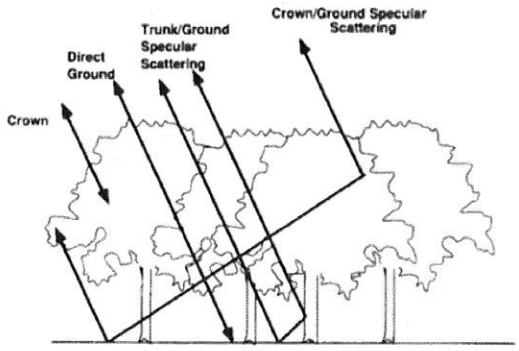

Fig. 8. Scattering mechanisms dominating σ° of forests.

stands consist of red maple, sugar maple, jack pine, red pine and grass-covered soil. The MIMICS input parameters are specified for these stands in Table I. The MIMICS model predicts net backscattering coefficient as the summation over various scattering pathways. The dominant terms for forests are depicted in Fig. 8, and at C-band include (1) direct backscatter from the crown layer of foliage and branches, (2) specular scatter at the ground interacting with the crown layer, (3) multiple specular scattering from the ground and trunks, and (4) direct backscatter from the ground. All terms are attenuated by passage through upper layers.

A summary of the MIMICS results for C-band with VV-polarization at $\theta = 22^\circ$ is given in Table II. MIMICS predicts an expected dynamic range of 6 dB between grass-covered soils and the mature hardwood stands of maple. The upland conifer stands are expected to have intermediate values of σ° which depend upon stand density and geometric properties of the crown layer. The partial contributions of various scattering pathways to σ° are also given in Table II. Scattering by the crown layer is found to dominate σ° for all forest types except for the immature red pine stand which is only 7.6 m in height. As a result, there is little expectation that the ERS-1 SAR can provide any information on soil moisture for mature forests in summer. In contrast, σ° from grass-covered soils is almost wholly determined by surface properties; and thus, σ° should be very sensitive to near-surface soil moisture.

B. Radar Backscatter Measured by ERS-1 SAR

The test stands selected for the MIMICS simulations are used to evaluate the MIMICS predictions. Each stand is identified within the calibrated ERS-1 scene and segmented. The values of σ° as averaged over all pixels in the stand are compared with the MIMICS estimates in Fig. 9. The estimates are found to agree with the measured values to within 1 dB except for the two northern hardwood stands. This modeling error for the hardwoods is probably related to a lack of appropriate branch geometry data for these species. Since no detailed measurements currently exist for maples, they have been assumed to have a branching architecture equivalent to that of aspens. Nevertheless, the overall agreement is excellent.

V. Land-Cover Classification

Both model and measurement show a difference of several

TABLE I
FOREST STAND CHARACTERISTICS USED BY MIMICS

	Jack Pine	Red Pine	Sugar/Red Maple	Red Maple
Ground Surface Properties				
Volumetric Soil Moisture (cm/cm)	0.027	0.027	0.045	.0.045
Soil Texture: % Sand	90	90	50	50
% Clay	0	0	10	10
RMS Roughness (cm)	1	1	1	1
Surface Correlation Length (cm)	15	15	15	15
Surface Model: SP = small perturbation	SP	SP	SP	SP
Trunk Layer Properties				
Mean Height (m)	15.3	7.6	12.8	15.2
Mean Diameter (cm)	15.51	13.59	9.82	10.12
Stem Density (stems/ha)	1 406	1 174	1 762	1 842
Dielectric Constant	20.4 -j5.1	21.9 -j5.9	20.0 -j4.9	17.8 -j3.7
Crown Layer Properties				
Crown Thickness (m)	6.00	6.10	6.61	8.31
Leaves Temperature (°C)	28	28	28	28
Mean Leaf Area (cm^2)	0.158	0.722	26.34	38.35
Mean Leaf Area Index (m^2/m^2)	5.38	4.13	3.80	3.72
Leaf/Needle Length (cm)	2.8	12.5	5.79	6.99
Leaf Thickness/Diameter (cm)	0.072	0.074	0.1	0.1
Leaf Density (leaves/m^3)	56 746	9 378	218	117
Leaf Moisture (g/g)	0.654	0.646	0.575	0.588
Dielectric Constant	15.3 -j5.1	14.9 -j5.0	16.0 -j5.2	16.7 -j5.4
Orientation (uniform = 0.5sinϕ)	0.5sinϕ	0.5sinϕ	0.5sinϕ	0.5sinϕ
Primary Branches				
Mean Length (cm)	50	73	200	200
Mean Diameter (cm)	0.75	0.99	1.5	1.5
Density (branches/m^3)	44.19	7.302	0.227	0.124
Dielectric Constant	20.4 -j5.1	21.9 -j5.9	20.0 -j4.9	17.8 -j3.7
Orientation	1.16sin(ϕ+41)^8	1.16sin(ϕ+41)^8	sin(ϕ+60)^9	sin(ϕ+60)^9
Secondary Branches				
Mean Length (cm)	25	33	100	100
Mean Diameter (cm)	0.50	0.57	0.75	0.75
Density (branches/m^3)	85.18	20.88	1.813	0.989
Dielectric Constant	20.4 -j5.1	21.9 -j5.9	20.0 -j4.9	17.8 -j3.7
Orientation	0.5sinϕ	1.52sin(ϕ+64)^16	sin(ϕ+60) ^9	sin(ϕ+60)^9

TABLE II
SUMMARY OF MIMICS RESULTS FOR VARIOUS LAND-COVER CATEGORIES AT *C*-BAND, VV-POLARIZATION AND $\theta = 22°$

Dominant Specie	Total		Percent of Total $\sigma°$		
	$\sigma°$(dB)	Crown	Crown/Ground	Trunk/Ground	Ground
Red Maple	-8.6	95.5	0.3	4.3	—
Sugar Maple	-8.9	96.4	0.4	3.2	—
Jack Pine	-10.7	100	—	—	—
Red Pine	-13.4	41.3	10.4	48.1	0.2
Grass	-14.4	0.03	0.2	—	99.8

dB between grass-covered soils and forests. However, is this sufficient to discriminate the two categories; and, furthermore, can various forest associations be machine discriminated as seems visually possible through examination of Figs. 2 and 7. To answer this question, $\sigma°$ is extracted from the calibrated ERS-1 imagery for many areas of known land-cover. A summary of the statistics for these regions is given in Table III.

Since machine classification must account for fading, the land-cover statistics of mean and standard deviation are calculated for both single (N = 6) pixels and 3×3 boxcar averages. The effective N of looks is calculated from the single pixel standard deviation to mean ratio assuming linear detection and Rayleigh fading statistics. For most categories, the effective N of looks is less than 6. This is a consequence of the measured standard deviation exceeding that predicted by Rayleigh fading; and implies that there is texture in the image related to within-stand and between-stand variance in $\sigma°$ for a given land-cover category.

Histograms of $\sigma°$ are shown in Fig. 10 for each land-cover category as described in Table III. The smooth surfaces of

TABLE III
SUMMARY OF ERS-1 IMAGE STATISTICS FOR VARIOUS LAND-COVER TYPES

Land-Cover Category		Number of Pixels	Effective Number of Looks	Single Pixel Statistics		Statistics for 3 x 3 Averages	
				Mean (dB)	Standard Dev. (dB)	Mean (dB)	Standard Dev. (dB)
Water: Inland Lakes		1 943	5.87	-26.37	1.96	-26.27	1.32
Concrete Runways		949	4.79	-22.79	2.14	-22.46	1.78
Grasses:	Prairie	718	4.99	-16.11	2.10	-16.00	1.49
	Hayfields	1 230	5.60	-15.18	2.00	-15.08	1.45
Upland Conifers:	Red Pine	1 943	5.71	-12.76	1.98	-12.66	1.42
	Jack Pine	2 044	5.53	-10.97	2.01	-10.80	1.32
Northern Hardwoods		2 206	4.73	-9.70	2.16	-9.59	1.54
Lowland Conifers:	All	3 824	5.57	-9.17	2.00	-9.05	1.37
	Spruces	3 293	5.34	-9.18	2.04	-9.06	1.39
	White Cedar	531	7.49	-9.09	1.75	-9.02	1.20

TABLE IV
LAND-COVER SEPARABILITY MATRIX FOR (A) A SINGLE-PIXEL CLASSIFIER AND (B) A 3×3 PIXEL CLASSIFIER

A. Single Pixel Classifier

		Inland Lakes	Concrete Runways	Grasses		Upland Conifers		Northern Hardwoods	Lowland Conifers		
				Prairie	Hayfields	Red Pine	Jack Pine		All	Spruces	Cedar
Inland Lakes											
Concrete Runways		0.87									
Grasses:	Prairie	2.53	1.57								
	Hayfields	2.83	1.84	0.23							
Upland Conifer:	Red Pine	3.46	2.43	0.82	0.61						
	Jack Pine	3.88	2.85	1.25	1.05	0.45					
Northern Hardwoods		4.05	3.05	1.51	1.32	0.74	0.31				
Lowland Conifer:	All	4.35	3.29	1.69	1.50	0.90	0.45	0.03			
	Spruces	4.30	3.26	1.67	1.49	0.89	0.44	0.12	0.01		
	White Cedar	4.66	3.52	1.82	1.62	0.98	0.50	0.16	0.05	0.02	

B. 3 x 3 Pixel Classifier

		Inland Lakes	Concrete Runways	Grasses		Upland Conifers		Northern Hardwoods	Lowland Conifers		
				Prairie	Hayfields	Red Pine	Jack Pine		All	Spruces	Cedar
Inland Lakes											
Concrete Runways		1.23									
Grasses:	Prairie	3.65	1.98								
	Hayfields	4.04	2.28	0.31							
Upland Conifer:	Red Pine	4.96	3.06	1.15	0.85						
	Jack Pine	5.85	3.76	1.85	1.55	0.68					
Northern Hardwoods		5.82	3.87	2.11	1.84	1.03	0.42				
Lowland Conifer:	All	6.40	4.26	2.43	2.14	1.29	0.65	0.03			
	Spruces	6.34	4.22	2.41	2.12	1.28	0.64	0.18	0		
	White Cedar	6.83	4.50	2.59	2.29	1.39	0.71	0.21	0.02	0.01	

inland lakes produce the lowest backscatter of approximately -26.4 dB. Relatively smooth concrete surfaces at airports have mean σ° only 3.8 dB higher at -22.8 dB. Natural prairie and hayfields should be easily discriminated from water and concrete with $\bar{\sigma}^\circ$ of about -15.5 dB (depending upon soil moisture and vegetation cover.) The forest categories cluster into two groups: (1) upland conifers with -12.8 dB $\leq \bar{\sigma}^\circ \leq$ -11 dB and (2) all other forest categories with $\bar{\sigma}^\circ \geq -9.7$ dB.

The expected accuracy of a Baysian classification can be estimated using the separability index S for two classes, i and j,

$$S = \frac{|\bar{\sigma}_i^\circ - \bar{\sigma}_j^\circ|}{SD_i + SD_j}$$

were $\bar{\sigma}^\circ$ and SD are the mean and standard deviation, respectively. For Gaussian distributions, values of $S \geq 1.5$ correspond to better than 90% correct classification. The computed values of S for the various land-cover categories are given in Table IV for both single-pixel statistics and those derived from the 3×3 boxcar averaging. The averaging process is shown to significantly improve separability. The use of filters larger than 3×3 do not add significantly to the 3×3 results.

These results show that, for a single summertime ERS-1 scene, all vegetated areas are easily discriminated from concrete and smooth water bodies. The grass-covered surfaces can be readily distinguished from all forested areas except red pine stands. Stands of northern hardwoods and lowland conifers cannot be readily separated and, furthermore, these stands will be partly confused with jack pine stands.

VI. SOIL MOISTURE ESTIMATION FOR GRASS-COVERED SOILS

It has been shown that grass-covered surfaces can be readily distinguished by ERS-1 SAR from the more densely vegetated forest areas and also that σ° from such surfaces is dominated

TABLE V
MIMICS INPUT PARAMETERS, σ° PREDICTED BY MIMICS AND σ° MEASURED BY ERS-1 SAR FOR GRASS-COVERED SOILS

	Prairie 1	Prairie 2	Prairie 3	Hayfield
Ground Surface Properties				
Volumetric Soil Moisture (cm/cm)	0.047	0.041	0.027	0.130
Soil Texture: % Sand	86.25	92.50	29.50	25.00
% Clay	2.50	0.00	5.00	46.25
Dielectric Constant	3.62 -j0.16	3.45 -j0.13	3.09 -j0.06	6.23 -j0.49
RMS Roughness (cm)	1.3	1.3	1.3	1.3
Surface Correlation Length (cm)	15	15	15	15
Surface Model PO = physical optics	PO	PO	PO	PO
Vegetation Properties				
Mean Grass Height (m)	20.9	19.2	12.6	67.9
Stem Density (stems/m^2)	1 818	2 161	644	662
Dry Biomass (kg/m^2)	0.664	0.563	0.145	0.954
Leaf/Needle Length (cm)	20.9	19.2	12.6	67.9
Leaf Width (cm)	0.6	0.6	0.6	0.6
Leaf Thickness/Diameter (cm)	0.1	0.1	0.1	0.1
Leaf Moisture (g/g)	0.154	0.128	0.442	0.440
Leaf Dielectric Constant	3.62 -j0.75	3.14 -j0.53	10.4 -j3.58	11.6 -j3.61
Air Temperature (°C)	28	28	28	28
Radar Backscattering Coefficients (dB)				
ERS-1 SAR	-16.1	— —	-17.5	-14.4
MIMICS (*C*-band, *VV*, 22°)	-16.3	-16.7	-17.9	-14.1

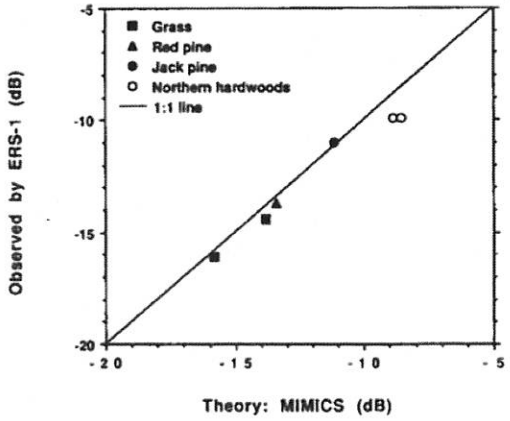

Fig. 9. Comparison of σ° measured by the ERS-1 SAR with that estimated by MIMICS.

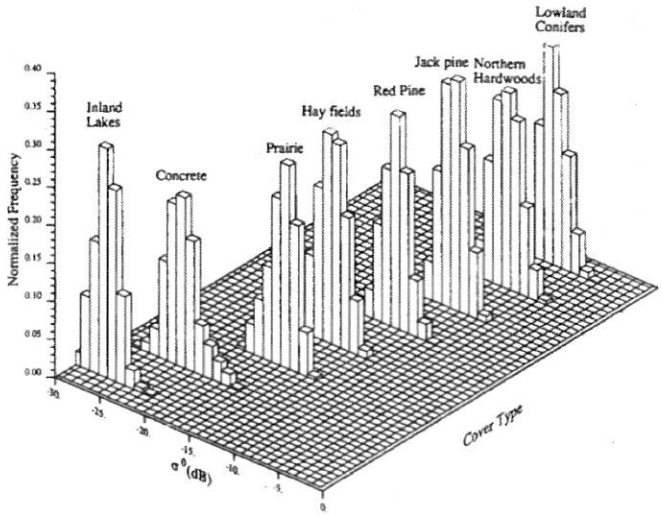

Fig. 10. Histograms of σ° observed by ERS-1 for various land-cover categories.

by surface properties (moisture and roughness). In order to estimate the utility of ERS-1 SAR for estimation of near-surface soil moisture, MIMICS simulations of σ° are compared to ERS-1 observations.

At the time of the ERS-1 overpass, four grass-covered areas were sampled. These areas include a hayfield and three prairie areas. Transects were used to acquire samples of soil texture, soil moisture, soil bulk density, grass height, biomass, and vegetation moisture content. These properties are summarized in Table V. Grass height is shown to vary between 19 and 68 cm and corresponds to variations in biomass of 145 to 954 g/m^2, respectively. Near-surface soil moisture in the upper 0–5 cm is shown to vary between 0.03 and 0.13 cm^3/cm^3.

MIMICS simulations of σ° as continuous functions of volumetric soil moisture are shown in Fig. 11 for both bare soil and a soil with a 40 cm thick grass cover. The surface scattering is calculated using physical optics with a RMS roughness of 1.3 cm and surface correlation length of 15 cm. For the grass-covered soil simulations represented by the solid line in Fig. 11, the vegetation parameters are held constant: grass height = 40 cm, dry biomass = 500 g/m^2, and vegetation moisture content = 0.44 g/g. The presence of this grass cover is expected to attenuate backscatter from the soil and reduce σ° by less than 0.2 dB. For both cases, the expected dynamic range of σ° is shown to be approximately 8 dB for soil moisture up to 0.25 cm^3/cm^3. This sensitivity is congruent with antecedent scatterometer and airborne SAR results [15, 16].

MIMICS estimates of σ° for each specific surface in Table V are also plotted as points in Fig. 11 along with associated σ° values derived from the calibrated ERS-1 data. The model results and ERS-1 measurements agree to within 0.4 dB for all cases. This excellent agreement demonstrates that retrieval of soil moisture from ERS-1 SAR is certainly feasible for surfaces covered with low biomass such as short grasses. The

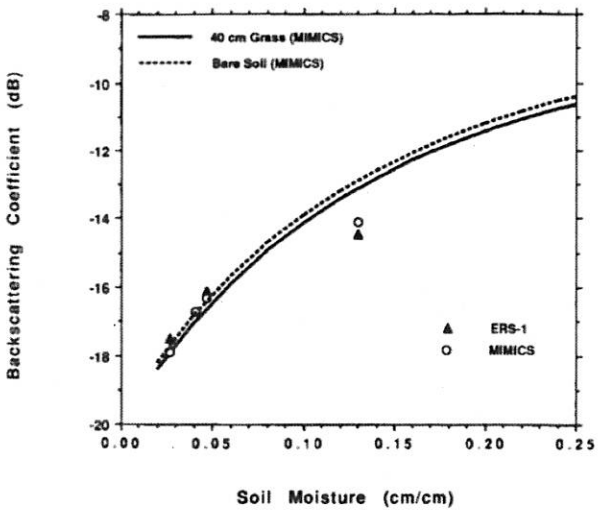

Fig. 11. Comparison of ERS-1 radar backscattering response to soil moisture with that expected by MIMICS. The lines represent hypothetical conditions modeled by MIMICS. The point symbols are for the specific conditions during the ERS-1 pass as described in Table V.

results also indicate that the quantity of biomass can lead to significant estimation errors (if not accounted for) as biomass approaches and exceeds 1 kg/m^2.

VII. Conclusion

This study demonstrates that ERS-1 SAR data is useful for several land applications. The preliminary calibration results indicate that across-swath variation in calibration offset is less than 3 dB as a consequence of antenna gain, R^4 losses and variation in A_i. The calibrated ERS-1 data for a single date in midsummer shows that limited discrimination and classification of land-cover categories are possible by machine processing. Such techniques need to account for fading by using appropriate filtering. The ERS-1 backscattering from forested areas is dominated by properties of the crown layer consisting of foliage and branches. Furthermore, ERS-1 SAR is sensitive to near-surface soil moisture for grass-covered soils, and soil moisture retrievals are possible. Finally, the multitemporal availability of ERS-1 SAR data holds exciting prospects for enhancing discrimination of vegetated regions by monitoring the seasonal changes in crown layer moisture and structure and for monitoring changes in near-surface soil moisture within regions of low biomass.

Acknowledgment

The authors gratefully acknowledge the contributions of Eric Wilcox, Ruben De La Sierra, and Kathleen Bergen at the University of Michigan and of Ian Brodie and Don Bragg at Michigan Technological University.

References

[1] F. T. Ulaby, B. Brisco, and M. C. Dobson, "Improved spatial mapping of rainfall events with spaceborne SAR imagery," *IEEE Trans Geosci. Remote Sensing*, vol. GE-21, pp. 118–121, Jan. 1983.

[2] B. Brisco, F. T. Ulaby, and M. C. Dobson, "Spaceborne SAR data for land-cover classification and change detection," in *IEEE International Geoscience and Remote Sensing Symposium (IGARSS'83) Digest*, Vol. II, Sec. PS-2, pp. 1.1–1.8, 1983.

[3] K. R. Carver, C. Elachi, and F. T. Ulaby, "Microwave remote sensing from space," *Proc.IEEE*, vol. 73, no. 6, pp. 970–996, 1985.

[4] M. C. Dobson and F. T. Ulaby, "Preliminary evaluation of the SIR-B response to soil moisture, surface roughness, and crop canopy cover," *IEEE Trans. Geosci.Remote Sensing*, vol. GE-24, pp. 517–526, 1986.

[5] J. R. Wang, E. T. Engman, J. C. Shiue, M. Rusek, and C. Steinmeier, "The SIR-B observations of microwave backscatter dependence on soil moisture, surface roughness, and vegetation covers," *IEEE Trans. Geosci.Remote Sensing*, vol. GE-24, pp. 510–516, 1986.

[6] J. B. Cimino, A. Brandani, D. Casey, J. Rabassa, and S. D. Wall, "Multiple incidence angle SIR-B experiment over Argentina: Mapping of forest units," *IEEE Trans. Geosci. Remote Sensing*, vol. GE-24, pp. 498–509, 1986.

[7] D. R. Brunfeldt, and F. T. Ulaby, "Active reflector for radar calibration," *IEEE Trans. Geosci. Remote Sensing*, vol. GE-22, pp. 165–169, Mar. 1984.

[8] D. A. Albert, S. R. Denton, and B. V. Barnes, *Regional Landscape Ecosystems of Michigan*. Ann Arbor, MI: School of Natural Resources, University of Michigan, 1986.

[9] Michigan State University Agricultural Experiment Station and Cooperative Extension Service in Cooperation with the U.S. Department of Agriculture Soil Conservation Service, *Soil Association Map of Michigan, Extension Bulletin E-1550, File 32.13*. Lansing, MI: Michigan State University, 1981.

[10] Michigan Department of Natural Resources, *Michigan Resource Information System (MIRIS): Chippewa County*. Lansing, MI: Land and Water Management Division, Michigan Department of Natural Resources, 1989.

[11] F. T. Ulaby, K. Sarabandi, K. McDonald, M. Whitt, and M. C. Dobson, "Michigan Microwave Canopy Scattering Model (MIMICS)," *Int. J. Remote Sensing*, vol. 11, no. 7, pp. 1223–1253, July 1990.

[12] S. T. Gower and J. M. Norman, "Rapid estimation of leaf area index in conifer and broad-leaf plantations using the Li-Cor LAI-2000," *Ecology*, vol. 72, no. 5, pp. 1896–1900, 1991.

[13] F. T. Ulaby and M. A. El-Rayes, "Microwave dielectric spectrum of vegetation, Part II: Dual-Dispersion Model," *IEEE Trans. Geosci. Remote Sensing,"* vol. GE-25, pp. 550–557, 1987.

[14] M. T. Hallikainen, F. T. Ulaby, M. C. Dobson, M. A. El-Rayes, and L. K. Wu, "Microwave dielectric behavior of wet soil - Part I: Empirical models and experimental observations," *IEEE Trans. Geosci. Remote Sensing*, vol. GE-23, pp. 25–34, 1985.

[15] F. T. Ulaby, P. B. Batlivala, and M. C. Dobson, "Microwave backscatter dependence on surface roughness, soil moisture, and soil texture: Part I - bare soil", *IEEE Trans. Geosci. Electron.*, vol. GE-16, pp. 286–295, 1978.

[16] A. Beaudoin, T. LeToan, and Q. H. J. Gwyn, "SAR observations and modeling of the C-band backscatter variability due to multiscale geometry and soil moisture," *IEEE Trans. Geosci. Remote Sensing*, vol. 28, pp. 886–895, 1990.

vfill

M. Craig Dobson (M'80–SM'91) received the B.A. degrees in geology and anthropology from the University of Pennsylvania, Philadelphia, in 1973 and the M.A. degree in geography from the University of Kansas, Lawrence, in 1981.

He is an associate research scientist at the University of Michigan. From 1975 to 1984, he worked at the Remote Sensing Laboratory of the University of Kansas Center for Research, Inc., where he managed several experimental programs related to microwave remote sensing of terrain. Specific research projects focused on the microwave dielectric properties of soils, microwave sensor response to soil moisture and crop canopy cover using truck-mounted and airborne scatterometers and radiometers, and multitemporal simulations of orbital SAR imagery. Since 1984, he has been with the Radiation Laboratory of the Electrical Engineering and Computer Science Department of the University of Michigan, where he conducts research on the microwave dielectric properties of vegetation and radar backscattering properties of forests.

Leland Pierce (S'85–M'85–M'89) received the B.S. degrees in both electrical and aerospace engineering in 1983, and the M.S. and Ph.D. degrees in electrical engineering in 1986 and 1991, respectively, all from the University of Michigan, Ann Arbor.

Since then he has been the head of the newly formed Microwave Image Processing Facility within the Radiation Laboratory in the Electrical Engineering and Computer Science Department at the University of Michigan, Ann Arbor, where he is responsible for research into the uses of Polarimetric SAR systems for remote sensing applications, specifically, forest canopy parameter inversion.

Kamal Sarabandi (S'87–M'90) was born in Tehran, Iran on November 4, 1956. He received the B.S. degree in electrical engineering from Sharif University of Technology, Tehran, Iran, in 1980. He received the M.S.E. degree in electrical engineering in 1986, and the M.S. degree in mathematics and the Ph.D. degree in electrical engineering in 1989, all from the University of Michigan.

From 1980 to 1984, he worked as a microwave engineer in the Telecommunications Research Center in Iran. He is presently an assistant research scientist in the Department of Electrical Engineering and Computer Science at the University of Michigan. His research interests include electromagnetic scattering, microwave remote sensing, and calibration of polarimetric SAR systems.

Fawwaz T. Ulaby (M'68–SM'74–F'80), received the B.S. degree in physics from the American University, Beirut, Lebanon, in 1964, and the M.S.E.E. and Ph.D. degrees in electrical engineering from the University of Texas, Austin, in 1966 and 1968, respectively.

He is currently Professor of Electrical Engineering and Computer Science at the University of Michigan, Ann Arbor, and Director of the NASA Centter for Space Terahertz Technology. His interests include microwave and millimeter wave remote sensing, radar systems, and redio wave propagation. He has authored several books and published over 400 papers and reports on these subjects. Dr. Ulaby has received numerous awards, including the IEEE Geosceince and Remote Sensing Distinguished Achievement award in 1983, The IEEE Centennial Medal in 1984, and the Kuwait Prize in applied science in 1986.

Terry L. Sharik received the B.S. degree in forestry and wildlife management from the Division of Forestry, West Virginia University, in 1964, and the M.F. degree in wildland recreation and the Ph.D. degree in forest botany from the School of Natural Resources, University of Michigan, in 1966 and 1970, respectively.

He is currently Professor of Forest Ecology at Michigan Technological University, where his research interests include population and community dynamics and the regeneration of forest trees.